Carbohydrate-carbohydrate interaction drives the preferential insertion of dirhamnolipid into glycosphingolipid enriched membranes.

Valeria Rondelli[1,#,*], Luca Mollica[1,#], Alexandros Koutsioubas[2], Nail Nasir[3,4], Marcus Trapp[5,6], Estelle Deboever[3,7,8], Paola Brocca[1], Magali Deleu[3,*]

[1] *Department of Medical Biotechnology and Translational Medicine, Università degli Studi di Milano, Italy*

[2] *Jülich Centre for Neutron Science at Heinz Maier-Leibnitz Zentrum, Forschungszentrum Jülich GmbH, Garching, Germany*

[3] *Laboratoire de Biophysique Moléculaire aux Interfaces, Structure Fédérative de Recherche Condorcet, TERRA Research Center, Gembloux Agro-Bio Tech, Université de Liège, Gembloux, Belgium*

[4] *Present address: Astel Medica SA., Tinlot, Belgium*

[5] *Gesellschaft für Anlagen- und Reaktorsicherheit (GRS) gGmbH, Schwertnergasse 1, 50667 Köln*

[6] *Helmholtz-Zentrum Berlin für Materialien und Energie, Institute for Soft Matter and Functional Materials, Hahn-Meitner-Platz 1, 14109 Berlin, Germany*

[7] *Laboratory of Natural Molecules Chemistry, Gembloux Agro-Bio Tech, University of Liège, 2, Passage des Déportés, B-5030 Gembloux, Belgium*

[8] *Present address : Neurodegenerative Research Center Tempe, Biodesign Institute, Arizona State University, United-State*

[#]The two authors equally contributed to the work

[*]Corresponding Authors:

Valeria Rondelli, valeria.rondelliunimi.it

Magali Deleu, magali.deleu@uliege.be

Keywords

model membrane, neutron reflectometry, SAXS, MD simulations, GM1 ganglioside

TOC

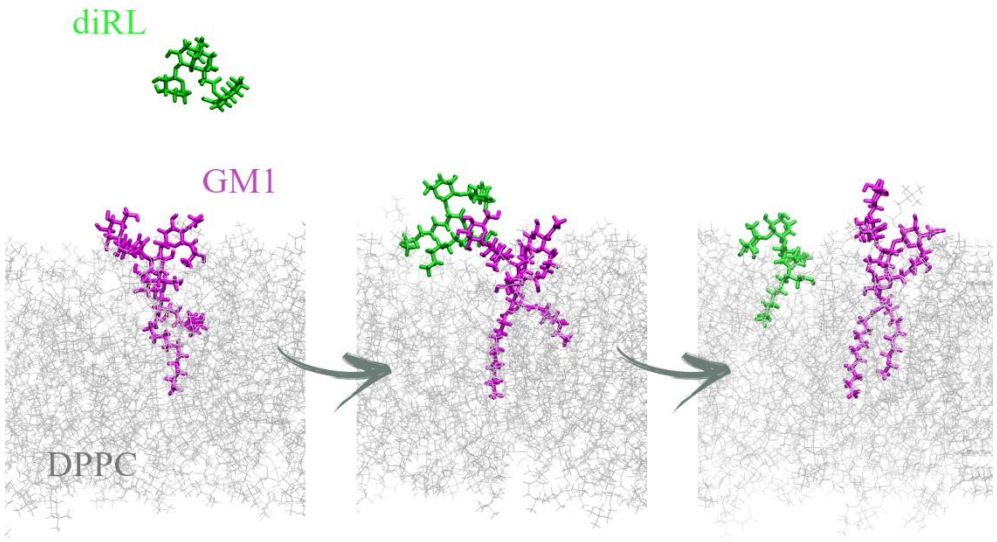

Abstract

Rhamnolipids (RLs) are among the most important biosurfactants produced by microorganisms, and have been widely investigated because of their multiple biological activities. Their action appears to depend on their structural interference with lipid membranes, therefore several studies have been performed to investigate this aspect. We studied by X-ray scattering, neutron reflectometry and molecular dynamic simulations the insertion of dirhamnolipid (diRL), the most abundant RL, in model cellular membranes made of phospholipids and glycosphingolipids. In our model systems the affinity of diRL to the membrane is highly promoted by the presence of the glycosphingolipids and molecular dynamics simulations unveil that this evidence is related to sugar-sugar attractive interactions at the membrane surface. Our results improve the understanding of the plethora of activities associated with RLs, also opening new perspectives in their selective use for pharmaceutical and cosmetics formulations. Additionally, they shed light on the still debated role of carbohydrate-carbohydrate interactions as driving force for molecular contacts at membrane surface.

Introduction

In the last years many studies have been dedicated to the discovery and use of biosurfactants due to their low toxicity, biodegradability and ecological safety. Among biosurfactants, rhamnolipids (RLs), composed by a hydrophilic anionic head group containing rhamnose and by two hydrophobic tails, hold a prominent position because of their interesting biological properties such as antimicrobial, antiphytoviral, zoosporicidal activities [1-4]. The most studied natural RLs are mono- and di-rhamnolipids (monoRL and diRL), having one or two rhamnosyl residues, excreted by various soil bacterial species such as *Pseudomonas* sp. and *Burkholderia* sp. [5]. The surfactant properties of rhamnolipids are well known: they reduce the surface tension of water and the interfacial tension of water/oil systems [6,7]. There is increasing interest in the effect of RLs on human and animal cells since RLs have been shown to affect cellular immunosuppression [8] and to display effects on human keratinocytes and fibroblast cultures [9]. Moreover, endotoxin-like properties have been described for RLs [10], which have also been assayed in the treatment of psoriasis [11] and in the process of cutaneous wound healing [12]. Thus, RLs have been proposed as vehicles for active ingredients in cosmetics and pharmaceutical applications [13]. Besides that, they also have a potential in plant protection as they are able to trigger the plant immune system conferring a better resistance to fungal pathogens [5,14, 15]. The intercalation of the RLs into the plasma membrane of target cells and the subsequent alteration of its physical properties has been proposed as a possible mechanism of their biological activity [16]. However, the detailed molecular mechanism of these interactions is still unknown. More particularly, their effect on lipid membrane domains, key platforms in signalling pathways, was poorly investigated. It is then of great interest to get insights into the nanoscale molecular level of the interaction of purified RLs with various lipid-based model membranes.

Several studies have been performed to investigate the effects brought by RLs to model lipid membranes, showing their importance in membrane stabilization or destabilization and in regulation of lipid polymorphism [17-19]. For example, the ability of RLs mixture to increase the fluidity of DPPC bilayers is parallel to the increase of vesicle permeation and may be related to the strong haemolytic power of these molecules [20,21]. Specifically, diRL has been shown to alter the physicochemical properties of neutral and charged phospholipid and plant mimic model membranes such as the mixtures phase behaviour, lipid order and packing and membrane thickness and permeabilization [16,22-25].

In this context, we focused on diRL, the major surfactant compound produced by *P. Aeruginosa*, and we studied from the structural point of view, its insertion in model membranes. *P. Aeruginosa* produces heterogeneous mixture of RLs, each of them, in principle, could have a different specific effect to host membranes. Therefore, disentangling individual contribution of each homologue to the biological properties of the mixture, is of interest. Such information would make possible the selection of RLs for formulations according to the specific need.

The step forward in the investigation of diRL interaction with models of cellular membranes that we present, is based on the use of mixed model membranes of phospholipids and gangliosides,

the latter belonging to membrane glycosphingolipids involved in several cell activities and signalling [26-29]. Since both diRL and the glycosphingolipid of the target membrane bear sugars in their polar portions, our study aims as well at the investigation of if and how carbohydrate-carbohydrate interactions play a role in the definition of membrane surface properties and on the ability of diRL to insert into the target membrane.

Our investigation has been performed by applying complementary experimental and computational techniques, such as small angle X-ray scattering, neutron reflectometry and molecular dynamics simulations.

Materials and methods

Lipids

Di-rhamnolipid (2-O-α-L-rhamnopyranosyl-α-L-rhamnopyranosyl-β-hydroxydecanoyl-β-hydroxydecanoate named diRL) was isolated from a commercial mixture of natural rhamnolipids from *P. aeruginosa* purchased from AGAE Technologies (AGAE Technologies, LLC, Corvallis, OR, USA). Therefore, a preparative high-performance liquid chromatography coupled to an evaporative light scattering detector (HPLC–ELSD) on an Interchim Uptisphere Strategy C18-2 column (21.2 mm, 15 µm) on an Interchim Puriflash 4250 system was used. Before injection, the mix was solubilized in pure methanol and filtered through a 0.22 µm PTFE membrane. Distilled water (with 0.1%, vol/vol, of formic acid) and acetonitrile (ACN) (with 0.1%, vol/vol, of formic acid) were used as mobile phase. For the first 8 min, the percentage of ACN was increased from 60% to 100% and maintained at 100%for 8 min. The percentage of ACN was decreased to 60% in 30 sec and the column was cleaned during 3 min. The flow was 20 ml/min. The purity of the diRL collected fractions was checked by HPLC-ELSD. The ELSD parameters were: 35 °C and 2.5 bars. The fractions with a purity higher than 95% were then pooled and dried with a speed Vac apparatus (10 mbar, 40°C). The samples were stored on the freezer (-20°C) in a hermetic box with desiccant until their use.

Cholesterol (purity ≥ 99%) has been purchased by Sigma-Aldrich. 1,2-dimyristoyl-sn-glycero-3-phosphocholine (DMPC – purity > 99%), 1,2-dipalmitoyl-sn-glycero-3-phosphocholine (DPPC – purity > 99%), 1,2-dipalmitoyl-d62-sn-glycero-3-phosphocholine (d_{62}DPPC – purity > 99%) have been purchased by Avanti Polar Lipid and used without any further purification. GM1 and GM3 gangliosides (purity > 99%) have been obtained according to [30] and [31] respectively.

Lipid target membranes preparation

Model lipid vesicles were prepared for SAXS experiments according to standard procedure described in [32] by thin film deposition and hydration. Extrusion through polycarbonate filters with controlled porosity of 80 nm was performed to obtain small unilamellar vesicles (SUV) composed by DPPC or by DPPC:GM1 (10:1 mol) at the final 30 mM concentration.

Single supported d_{62}-DPPC and d_{62}-DPPC:GM1 (10:1 mol) membranes for neutron reflectometry experiments have been prepared by the vesicle fusion technique [33] after dilution of the vesicles to the 1 mM concentration, while the three component d_{62}-DPPC:cholesterol:GM3 ganglioside (10:2:1 mol) membrane has been obtained by the fusion of d_{62}-DPPC-cholesterol vesicles and subsequent GM3 ganglioside incubation following the protocol described in [32].

SAXS

Small Angle X-Ray Scattering (SAXS) experiments have been performed at the ID02 beamline at ESRF, Grenoble [34]. The sample to detector distance was set to 10 m and 1 m, allowing to investigate a q-range between 0.01 and 6 nm^{-1}. Target membranes and diRL solution have been prepared at the 30 mM concentration and put in polycarbonate capillaries for measurements. For the mixing measurements diRL solution was brought to 3 mM concentration and mixed to SUV solution to the final lipid:diRL 95:5 molar proportion. In particular, 46 µL of a diRL solution at 3 mM concentration, have been added to 100 µL of the target vesicles solutions at 30 mM concentration. Three temperature conditions were investigated, corresponding to the lipid gel phase at 26°C, the fluid phase at 50°C and again back to the gel phase at 26°C. After data normalization, capillary and buffer contributions were subtracted from samples spectra. Data have been analyzed using the software SasView [35].

Neutron Reflectometry

Neutron reflectometry (NR) measurements on GM1 containing membranes have been carried out on MARIA beamline [36] operated by Jülich Centre for Neutron Science at Heinz Maier-Leibnitz Zentrum in Garching (Germany), using custom temperature-regulated liquid cells [37]. Measurements were performed using two wavelengths: 10 Å and 5 Å, with 10% wavelength spread.

NR measurements on GM3 containing membranes and on base phospholipid membranes have been performed on the V18 reflectometer at HZB [38] (Berlin, Germany) in TOF mode, $2 < \lambda < 12$ Å, with three incoming angles, 0.5°, 1° and 2.8°, and wavelength resolution $\Delta\lambda/\lambda = 5\%$. Sample cells were oriented vertically, and measurements were performed at the silicon-water interface, the beam coming from the side of the silicon block, at 25°C.

In a NR experiment, a grazing neutron beam is sent to a stratified sample, and the interference of the beam portions reflected at each interface are collected as a function of the momentum

transfer q. When the reflection is specular, the variation of the wave vector occurs in the surface normal direction, that is z, allowing to describe the sample in the cross (z) direction. In such NR experiments, the outcome is the sample scattering length density (SLD) profile along the z direction, also called $\rho(q_z)$, which depends on the chemical composition of the investigated materials along the normal. Called b_i the coherent nuclear scattering lengths of the sample constituent atoms, and their number along the surface normal direction n_i,, $\rho(q_z) = \sum_i b_i n_i$. The variation of reflected intensity as a function of momentum transfer $R(q_z)$ is related to the square modulus of the one-dimensional Fourier transform of $\rho(q_z)$ through the relation:

$R(q_z) \sim (16\pi^2 / q_z^2)|\rho(q_z)|^2$

Data have been analyzed using the programs MOTOFIT [39] and anaklasis [40]. Data collected in different solvents have been co-refined with the same structural model, in order to reduce the ambiguity of the obtained parameters. After analyzing the data referred to the bare target membranes and extraction best fit parameters, data referred to the membranes after incubation of diRL have been analyzed by imposing the same lipids volume fractions and by letting the leaflet SLD change according to the values reported in Table S1 of the Supporting Information, in order to evaluate diRL incubated amount.

MD simulations of DPPC and DPPC-GM1 bilayers and of diRL

The starting structure of the DPPC bilayer, constituted of 128 (64+64) molecules has been downloaded alongside the latest version of the SLipids force field [41-42]. The original water molecules have been removed and the bilayer has then been used for the creation of the DPPC-diRL and DPPC-GM1-diRL systems for MD simulations.

Topologies for the molecular dynamics simulations (MD, see further) for the diRL and GM1 molecules have been generated manually drawing their structures in Avogadro [43] (with GM1 adapted from the one present in the structure of endoglycoceramidase I, PDB ID 5J7Z) [44], then computing it using the generalized Amber [45] force field atomic names and parameters (in order to make them compatible with the lipid molecules parametrization used for DPPC) integrated with carbohydrate extension GLYCAM06 [46] as implemented in AmberTools [47]. Due to the size of the molecules we have used the semiempirical AM1-BCC [48] approach for determining the molecular partial charges, that has been demonstrated in the past to be potentially equivalent to the quantum-chemistry based RESP approach in handling the chemistry of carbohydrates and their interactions. The Amber topology has been transformed for its usage in GROMACS (see further) using Acepype [49].

MD simulations have been performed with the GROMACS software suite [50] on system that have been manually built within its framework of utilities. DPPC-diRL system has been built moving from the original 128-molecules bilayer and manually placing two molecules of diRL in a 57 x 57 x 148 $Å^3$ box with the bilayer center of mass coinciding with its geometric center and its longitudinal

axis parallel to the z axis of the simulation box, then the box has been filled with 10622 molecules of water using the TIP3P model [51].

DPPC/GM1-diRL system has been built as previously described, but 6 molecules of GM1 have been properly oriented and inserted in the bilayer (3 molecules for each side of the membrane model) adopting a molecular volume that allowed the removal of DPPC molecules incompatible with the volume of the GM1 molecule. This led to the construction of a 57 x 57 x 149 $Å^3$ system composed of 91 molecules of DPPC, 6 molecules of GM1, 6 Na+ ions (for the balance of GM1 single negative charge) and 11170 molecules of TIP3P water. The GM1/DPPC ratio almost corresponds to the experimental relative concentration (10%). A representation of the simulation box is reported in Figure S1.

The system size and set up, including the time extension of the simulations, have been chosen in order to identify and investigate the atomic-level details of the hydrophilic and hydrophobic driving forces that modulate the interactions between diRL and GM1. We opted, as a compromise between accuracy and computational cost, for a system size suitable for focusing on these details on timescales compatible with the diffusional properties of diRL in water, the stabilization of novel interactions between diRL molecules and the components of the membrane.

Each system has been minimized with the steepest descent method with a 0.01 energy step and water molecules that had fallen (< 100) during the building phase in the hydrophobic core of the bilayer have been removed with a simple script. The systems have been then minimized again and equilibrated from -263°C to 26 °C and to 50 °C in 10 ns in the NVT ensemble, using the V-rescale algorithm for temperature control [52] and with a 2 fs integration step and the long range electrostatics treated with the Particle Mesh Ewald method [53] and isotropic periodic boundary conditions.

The equilibrated structures have then been used for running 6 MD simulations at 26 °C and 6 MD simulations at 50 °C, each one of 75 ns, in order to improve the statistical relevance of the interactions of diRL with the double layer of DPPC.

As internal reference (data not shown) 50 ns MD simulations (at 26 and at 50 °C) of diRL and of GM1 in solution, of a DPPC bilayer and of a DPPC-GM1 bilayer have also been performed using the same parameters listed above. Moreover, GM1 and diRL simulations have been performed at different solute concentrations, i.e. 1, 2 and 6 molecules in the simulation box. All the simulations led to numerically stable run, with no loss of GM1 from the bilayer in the DPPC-GM1 system and expected aggregation of GM1 and diRL in solution.

Results and discussion

The effects of DiRL biosurfactant in lipid-based model membranes with varying composition was investigated to establish if the presence of membrane domains within host membranes makes their inclusion more favourable and to get insights on the structural consequences brought by its

inclusion in the lipid membranes. The complementary use of different experimental models and biophysical techniques allowed to unveil diverse aspects of the interaction.

Two target systems have been explored: a) pure phospholipid membranes and b) glycosphingolipid-containing phospholipid membranes. Glycosphingolipids were specifically chosen from the ganglioside family, fundamental lipid components in functional membrane domains.

For the experimental part, we dealt with two membrane geometries: i) diRL incubated in preconstituted planar membranes ii) diRL incubated in preconstituted membranes with a proper curvature.

1. diRL incubation in planar membranes

Neutron reflectivity from supported bilayers is a focused scattering technique appropriate for measuring diRL propensity of interaction with model membranes. The method consists in bringing, from the bulk solvent, diRL in contact with a model bilayer deposited on a few cm^2 sized silicon support at room temperature. Supported membranes offer to the incoming molecules a planar interface without macroscopic curvature, hard to be penetrated. Different bilayer compositions were addressed and diRLs were incubated at the final lipid:diRL 95:5 molar proportion. After incubation, we studied the final membrane structure in a comparative perspective with the original bare bilayer. Deuterated phospholipids have been used, to exploit the sensitivity of neutrons to isotopes and enhance the visibility of diRL upon insertion.

In the bulk solvent diRL was at 1 nM concentration, well under the cmc (100 μM). This experimental condition helped in stressing the detection of even minor effects.

Figure 1 reports the outcomes of NR investigation on mixed phospholipid-ganglioside, d_{62}DPPC-GM1 membranes showing how the neutron SLD transverse profile changes after contact with the diRL solution. On the contrary, even after 12h for incubation, diRL did not even slightly modify the pure d_{62}-DPPC membrane (See Fig. S2). Very interestingly, results reveal that the interaction of diRL with membrane was not ubiquitous but was solely observed when glycosphingolipids were present in the target bilayer. Come and coworkers[54], previously reported a higher affinity of RLs mixtures with cholesterol and sphingomyelin containing lipid membranes, but the interaction with gangliosides of the sole diRL was never investigated before. However, the insertion of diRL in the ganglioside-containing membrane did not bring major structural alteration to the bilayer parameters, as reported in Table 1.

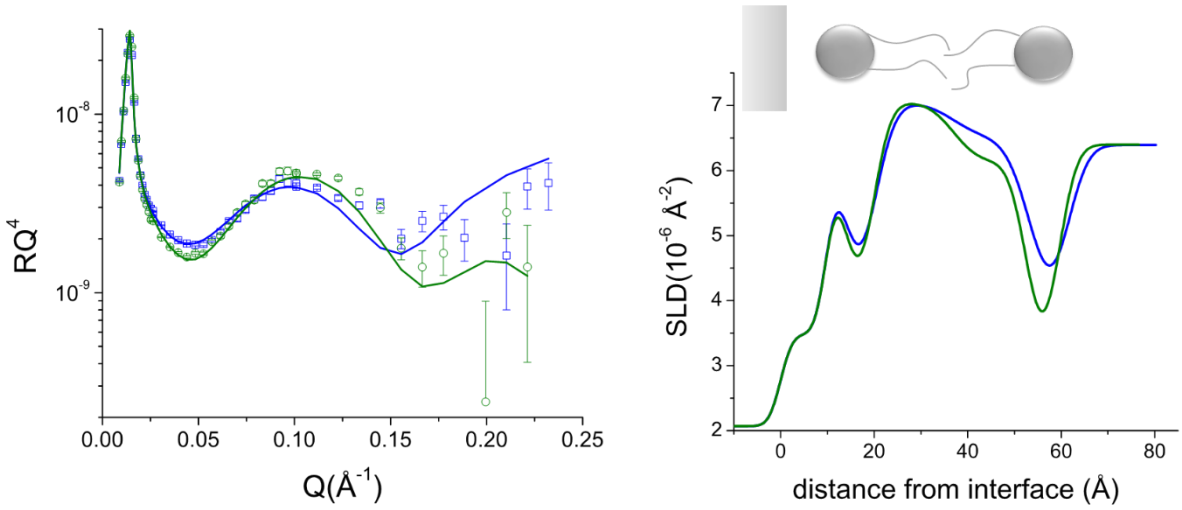

Figure 1 ***NR from ganglioside containing membrane in interaction with diRL.*** Left) Neutron reflectometry curves (symbols), together with their best fit (lines) relative to the d_{62}DPPC-GM1 membrane before (blue) and after (green) the interaction with diRL. Right) SLD profiles obtained from best fits. The drawing drives the eye in SLD interpretation. Data have been collected at room temperature.

Table 1 Physical parameters corresponding to the best fits of the reflectivity curves of the d_{62}-DPPC -GM1 membrane before and after diRL incubation at room temperature. T: layer thickness (±0.5 Å); $\rho_l(z)$: average scattering length density of the non-water components of the layer (±0.02 10^{-6} Å^{-2}); W: percent water content of the layer (±4% in volume); r: roughness between one layer and the adjacent previous one (±1 Å); %diRL: volume percentage occupied by diRL calculated by $\rho_l(z)$ variation.

	d_{62}DPPC-GM1				**d_{62}DPPC-GM1 + diRL**				
	T	**$\rho_l(z)$**	**W**	**r**	**T**	**$\rho_l(z)$**	**% diRL**	**W**	**r**
water	5			3	5				3
Heads in	5	1.93	21	4	5	1.93		21	3
Chains in	18	7.19	18	4	18	7.19		18	4
Chains out	16	6.53	18	4	17	6.53	6.6%	18	3
Heads out	6	1.76	22	4	6	1.76	6.6%	21	3

Beside the information about the preferential interaction with glycosphingolipid containing membranes, this experiment sheds light also on the impact of diRL on membrane stability. In fact, during reflectivity experiments, membranes have been first prepared and characterized in different contrast solvents (based on D_2O and H_2O mixtures), then diRL were incubated to the membranes from the bulk. Reflectivity was measured again after the needed time for equilibration of the system and, finally, solvents were drop by drop substituted (procedure called 'solvent exchange') to collect again reflectivity of the final system in different contrast solvents, in order to minimize the freedom degrees in data fitting and interpretation.

Data collected after diRL addition in the first solvent, the one in which diRL was incubated, are consistent with diRL insertion in the outer membrane leaflet without additional solvent penetration across the bilayer. But then, the small perturbation caused by the drop by drop solvent substitution induced membranes destabilization and high increase in solvent penetration, impeding a multiple-contrast investigation of the final membrane. This membrane disruption is likely to be connected to the high local curvature that diRL is willing to induce to the host planar membrane, as previously found by other authors who studied the effect of monoRL and diRL mixtures to POPC-based membranes [54]. In our experimental condition the environment is more challenging, since a curvature-inducing molecule that is GM1 ganglioside is already inserted in the target membrane.

To deepen the investigation of this induced instability, we repeated the experiment on a further more complex membrane: a three component d_{62}DPPC-cholesterol-GM3 ganglioside supported bilayer was prepared as a target to diRL interaction. GM3 ganglioside is analogous to GM1 but, bearing only three sugar units in its headgroup at the place of five, has a packing parameter, at the border between curved and flat aggregates forming lipid. Results, reported in SI (Figures S3 to S5 and table S2), confirmed the same trend observed in the DPPC-GM1 targeted membrane: diRL does insert in the outer leaflet (with no cholesterol redistribution between leaflets) and the final water flushing destabilized the membrane.

Clearly, the presence of sugars on the target systems bridged the diRL affinity to membranes, but the membrane results to be deeply altered, being high the amount of solvent at the distances from the solid support where usually the hydrophobic core of the membrane is found. In fact, membrane destabilization may be due to a role of diRL in the production of defects for solvent penetration, connected to the previously demonstrated ability of diRL to enhance membrane local curvature [19,54], driving to rupture when the membrane is mechanically stressed.

Here, we technically exploited reflectometry from single supported membranes, to unveil precise membrane interaction affinity for surfactants, otherwise difficult to address. On the other hand, supported bilayer studies constitutionally suffer the influence of the silicon substrate that may induce some spurious effects. Nevertheless, the condition of having one supported membrane can be the way to emphasize some key aspects of diRL behaviour, not sensed in more rearrangeable structural set ups.

Given the proved affinity of diRL for sugar-enriched membranes, which does not depend on the presence of cholesterol, we extended the study by performing a bulk investigation of diRL/membrane interaction using vesicular systems. In bulk, response will be highly averaged and may present higher complexities, but will allow to overcome the restriction of the solid support giving the opportunity to eventually corroborate the obtained result.

2. diRL interaction with vesicular model membrane.

The second experimental part of our study was therefore devoted to the investigation of the structural consequences for the target membrane when diRL coming from the external environment interacts with not-supported model membranes. The investigation has been performed by small angle X-ray scattering (SAXS) on large unilamellar vesicles (LUVs).

To gain in visibility, the interaction occurs between a solution of diRL in their aggregated phase at 3 mM concentration (above the cmc, 100 µM) and a 30 mM concentrated solution of vesicles. Fig 2 panel a) reports the SAXS profile of concentrated diRL in solution consistently fitted (See SI, Table S3) by the form factor of a bilayer 3 nm thick. Objects prevailing in the scattering profile extend up to at least 900 nm in size, that is the limit of size accessible with the used experimental sample-to-detector distance, determining the accessible q-range. At the lower concentration of 3 mM, the one at which diRL was diluted for the mixing experiments, diRL aggregates in structures with lower dimensionality visible from the slope at low q-vectors (See SI, Figure S6). The aggregative behaviour observed in solution is in agreement with the literature, where several authors report a concentration dependent aggregative behaviour of diRL in different pH and ionic strength conditions [21,55].

We investigated two vesicular systems: a pure DPPC membrane and a DPPC:GM1 10:1 mol one, analogous in composition to the supported membrane systems studied by NR, and two temperatures, 50°C and 26°C giving rise respectively to a fluid and gel phase of DPPC. SUVs and diRL solutions were mixed to the final lipid:diRL 95:5 mol proportion.

Despite diRL have been let to interact with the membranes at room temperature, where the lipid chains are in the gel phase, mixing was observed to be very fast in both systems and no evolution was observed during measurements. Both the mixed systems and the diRL solution have been investigated at different temperatures and no annealing effect was observed as no effect of temperature was noted on diRL aggregates curves collected at 26°C before and after bringing the system to 50°C.

SAXS data collected for the systems at 50°C before and after diRL interaction are reported in panels b) and c) of Figure 2 for a comparison, while the data at 26°C and 50°C are reported in panels d) to m) together with their best fits.

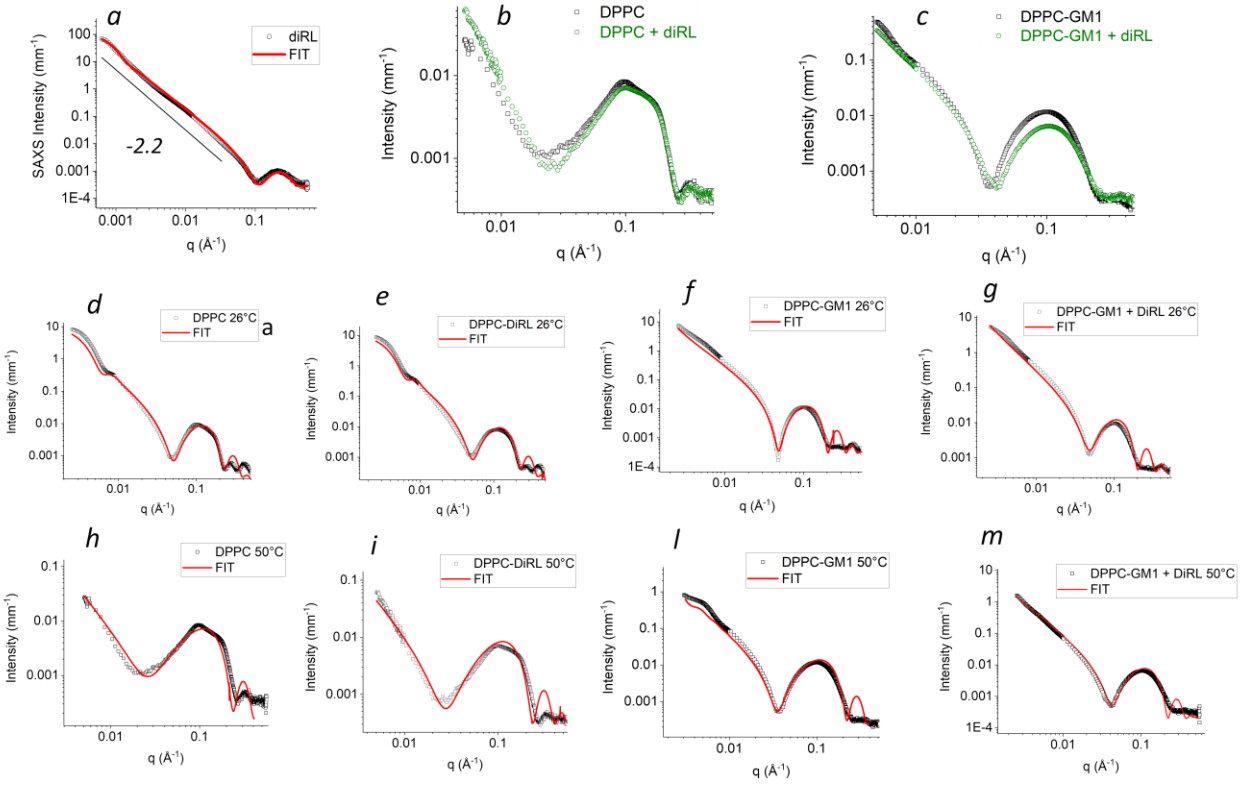

Figure 2 ***diRL incubation in vesicles***. *a)* SAXS curves of diRL aggregates at 30 mM concentration; b) SAXS from DPPC vesicles before (black) and after (green) the incubation of diRL, collected at 50°C; c) SAXS from DPPC-GM1 vesicles before (black) and after (green) the incubation of diRL, collected at 50°C. Panels from d) to m) report the SAXS profiles (black) of the DPPC and DPPC-GM1 vesicular systems investigated before and after diRL incubation at the different temperatures, with their best fits (red lines).

DPPC vesicles present a modulation of SAXS profile in the region of the bilayer form factor, that can be originated by a residual membrane staking after extrusion, while after diRL incubation the bilayer form factor region has a smoother curvature. However, the *1,2* periodicity is not easily recognizable, and the second repetition region is conserved after diRL interaction. Moreover, the well-defined minimum of the form factor of the whole vesicles in the low-q region, is perfectly reproduced after incubation of diRL (see Figure 2 panel d and e at 26 °C where low-q spectra is visible). Multilamellarity and its alteration by surfactants would manifest most likely in smearing out and enhancing of this modulation[56], respectively, which is not occurring here.

The shape of SAXS curves may be symptom of system with some surface faceting known to occur in DPPC vesicles especially at low temperature,[57-58] eventually smoothed by small surfactant insertion. Another interpretation of DPPC form factor modulation consists in considering vesicle-vesicle close interaction, also named docking phenomenon, known to occur in phospholipid LUVs [59]. Quantitatively, the relevance of docking would depend on solution conditions and, in the present case, could be tuned by altered physical parameters when diRL is present, screening membranes interaction, thus leading to a decreased modulation of the form factor.

When SAXS data are fitted by a spherical 3 shells model (internal heads, lipid chains and external heads) with a water core, the obtained scattering length density profiles (see SI-Figure S7) are consistent with the hypothesis of vesicular system with asymmetric bilayer, being the electron density of the external heads slightly higher than that of pure DPPC. It appears that fusion between diRL large aggregates and the DPPC vesicles hardly occurred and, having waited for system equilibration, also monomer exchange processes, have been allowed.

On the other hand, in DPPC-GM1 vesicles system, we found that diRL incubation affects membrane structure in a more evident manner. The whole membrane density and scattering length density (see SI-Figure S7) is affected by diRL presence. The membrane hydrophobic portion thickness being slightly reduced and the whole system has a less defined size (the spectrum of the system in the low q region does not show interference related aggregate size in the diRL containing systems) at high temperature.

In both systems an effect of diRL in disturbing membrane structuring is observed but the effect depends on the membrane domain they attach.

To obtain molecular details about the interaction between diRL and ganglioside-enriched membrane, we performed molecular dynamic (MD) simulations.

MD simulations

In order to elucidate the different behavior of diRL molecules as a function of GM1 concentration on the surface of DPPC double layers, we performed molecular dynamics (MD) simulations of diRL-DPPC-water and diRL-DPPC/GM1-water in the NVT canonical ensemble. Each of these simulations has been performed six times for a total simulation time of 75x6 = 450 ns with the aim of monitoring the statistical relevance of the interactions. Moreover, two different temperatures have been monitored, i.e. T = 26 °C and T = 50 °C, respectively corresponding to the gel phase and fluid phase of DPPC membranes.

We have monitored the different propensity of diRL for the binding to DPPC through hydrophobic interactions in presence or absence of GM1, i.e. its ability to immerse its hydrophobic chains into the hydrophobic core of DPPC double layers. In this respect, we divided the molecules of interest in a hydrophobic and in a polar part (Figure 3, panel a) in order to analyze all the combinations of their interactions during the MD simulations.

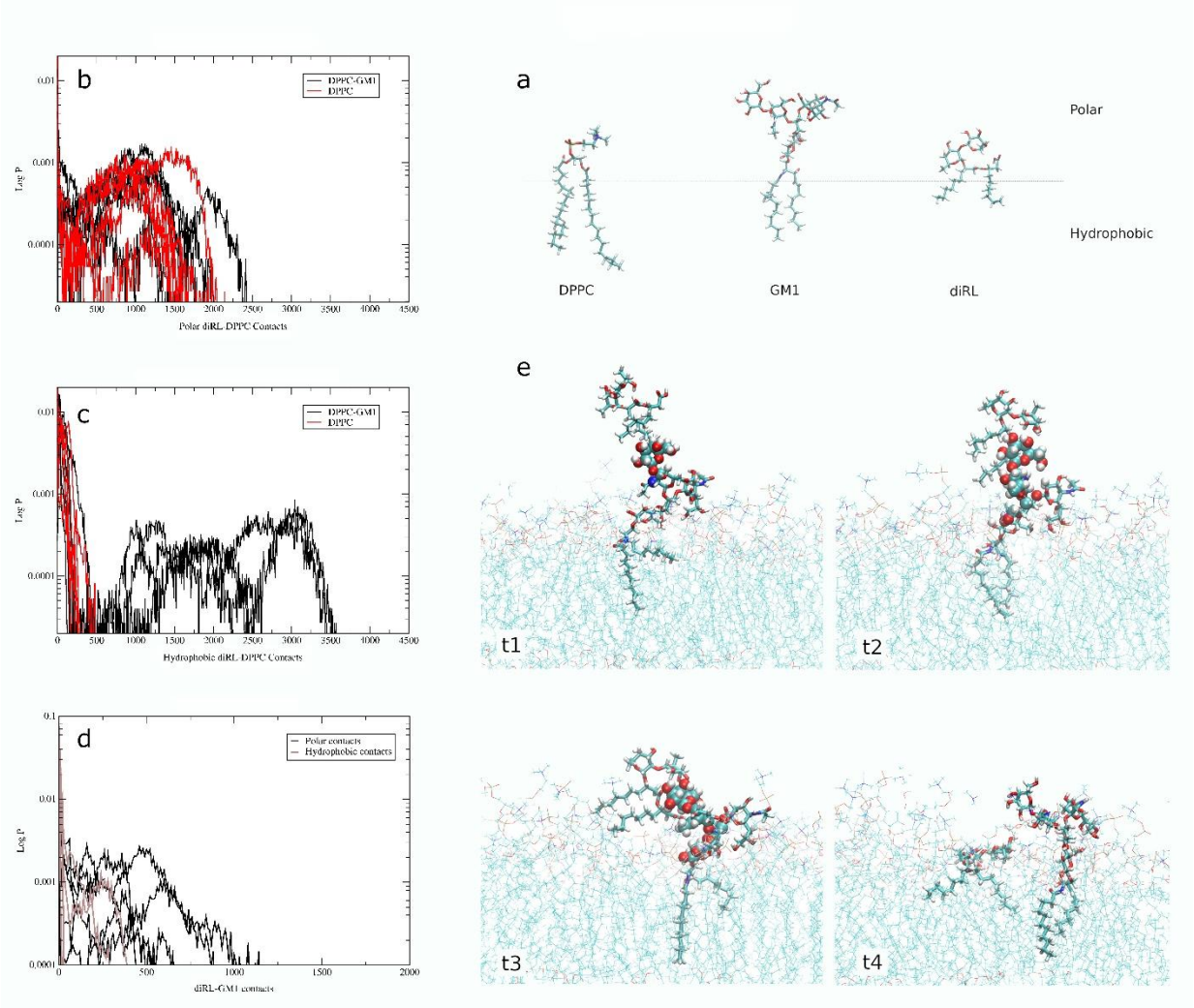

Figure 3 a): Regions of DPPC, GM1 and diRL molecules as reported in the main text, i.e. identified according to their interactive propensity (of polar and hydrophobic type) with other molecular partners; b) and c): Distributions at 26 °C of polar (b) and hydrophobic (c) contact probability (in logarithmic scale) between diRL molecules and DPPC molecules in DPPC-GM1 (in black) and DPPC only (red) double layers; d): Distributions of polar (black) and hydrophobic (brown) contact probability between diRL molecules and GM1 molecules in DPPC-GM1 bilayers; e) example of the progressive insertion (t1<t2<t3<t4, t4-t1 = 40 ns) of diRL in the DPPC-GM1 bilayers after a first contact between diRL and GM1 (t1), the stabilization of polar contacts between them (t2), the protrusion of diRL hydrophobic chains toward the inner core of DPPC-GM1 bilayer while polar contacts are still anchoring the molecules together as well as with the surrounding DPPC molecules (t3) and eventually the detachment of diRL from GM1.

The statistical analysis of the diRL-DPPC polar and hydrophobic contacts evidenced a net different behavior: the former probability distribution at 26 °C for DPPC and DPPC/GM1 double layers is almost identical (Figure 3, panel b), whereas the latter changes dramatically (Figure 3, panel c) when GM1 is included in the DPPC membrane, with no DPPC-diRL hydrophobic interactions occurring in absence of GM1 and a huge number of them occurring when GM1 is present.

Moreover, we have analyzed the same type of contacts in the diRL-GM1 interactions (Figure 3, panel d), revealing that the vast majority of them are polar, i.e. they occur through sugar-sugar interactions. All these data taken together suggest that when GM1 is not present on the surface of DPPC membranes the interaction between diRL and DPPC is the one between phospholipids polar heads and the sugar moieties of diRL. When present (Figure 3, panel e), GM1 sugar units transiently interact (t1, t2, see also Table 2) with the ones of diRL allowing its hydrophobic chains to protrude toward the double layer inner core (t3), then driving the diRL dissociation from GM1 and its miscibility in DPPC (t4). The analysis of computed times in the MD simulations timescale (Table 2) reveals a homogeneity of diRL-DPPC contact duration (40-50 ns on average) with or without GM1 despite a different type of interaction occurring in the system, with the diRL-GM1 contact time much shorter (about 50%) in statistical agreement with the mechanism proposed.

Table 2 Largest residence times observed during the single replicas of the simulations, each one consisting of the same system with the same number of particles (N), constant volume (V) and temperature (T) with different initial velocities distribution (i.e., different random seed). Two different temperatures have been used, i.e. T = 26 °C and T = 50 °C (See SI- Figure S8). The times are expressed in nanoseconds: the ones indicated in gray are the longest ones observed during the simulation in presence of more than one association/dissociation event.

Replica	DPPC		DPPC-GM1			
	CONT: diRL-DPPC		CONT: diRL-DPPC		CONT: diRL-GM1	
	T = 26 °C	T = 50 °C	T = 26 °C	T = 50 °C	T = 26 °C	T = 50 °C
1	47	60	70	70	68	5
2	30	35	50	20	10	60
3	41	75	50	50	40	15
4	50	50	35	50	18	55
5	74	60	60	50	16	18
6	10	30	9	22	23	10
Average	42	52	46	44	29	27
St.Dev.	21	17	21	19	24	24

General Discussion and Conclusion

DiRL is a biosurfactant with unique biological properties. The hypothesis is that the properties inferred by RLs to the host membranes and aggregates they are part of, depend on their structural properties on one side and on the way they contact the molecular species constituting the membrane bilayer[16]. We addressed for the first time diRL brought into contact with model membrane from diluted/rich water solutions, following an incubation time in the range of hours and by MD simulations. The work proceeded in a comparison between diRL propensity to interact

with phospholipid bilayers and with gangliosides (in particular of GM1 ganglioside) enriched phospholipid bilayers.

Globally, results show the relevant role of glycosphingolipid in mediating the insertion of dirhamnolipid into phospholipids.

We unveiled that diRL has a preference for sugar containing interfaces where it induces membrane thinning, increases membrane fluidity and augments local membrane curvature.

We unveiled as well that the driving force for diRL insertion in ganglioside-enriched membrane is carbohydrate-carbohydrate interaction.

If and how sugar-sugar interactions play a role in the definition of membrane surface properties in the presence of the two charged glycolipids of the same charge sign, is an interesting point. Carbohydrate-carbohydrate interactions have been largely suggested and demonstrated [60-66] to play a role in the affinity of two facing surfaces, finely governing cell-cell recognition and adhesion.

In our framework of facing a small sugar headed lipid (diRL) with a larger one, having hindrance requirements (GM1) that locally imposes a curvature to the membrane and that is suggested to easily clusterize [67], made the issue even more difficult. Considering the GM1-enriched vesicle surface has a charge-decorated surface, some kind of reentrant condensation effect may be considered as the robust lock-key mechanism for augmented affinity [68] already observed to bring lipid aggregates with the same charge to feel attractive forces on very short distances [69].

Notably, supported membranes and neutron reflectometry have been exploited as a new tool for studying such preferential interactions otherwise difficult to be addressed.

Besides the interest of the presented results from a fundamental point of view, the novel information contained in the present work may be profitably used for the development of diRL-based drug delivery systems, suggesting membrane carbohydrate components as possible sites of interaction for rhamnolipids.

Authors' Contributions

Valeria Rondelli: conceptualization, NR, SAXS, writing **Luca Mollica:** MD, writing **Alexandros Koutsioubas:** NR, writing **Nail Nasir:** conceptualization, NR, writing **Marcus Trapp:** NR, writing **Estelle Deboever:** NR, writing **Paola Brocca:** SAXS, writing **Magali Deleu:** conceptualization, NR, writing

Acknowledgements

This project has received funding from the European Union's Horizon 2020 research and innovation programme under grant agreement No 731019

(EUSMI). This research was partly funded by the 'Medical Biotechnology and Translational Medicine Department' of the 'Università degli Studi di Milano', grant number 'PSR2018' and 'PSR2020' to V.R.

The authors thank the Belgian Fund for Scientific Research (F.R.S.-FNRS) for its financial support via the CDR Project J.0086.18 and the University of Liège for its support via the ARC-FIELD project 13/17-10.

The authors thank the instrument teams of MARIA, Jülich Centre for Neutron Science (JCNS) at Heinz Maier-Leibnitz Zentrum (MLZ, Garching, Germany) of V18 reflectometer at HZB (Berlin, Germany) and of ID02 beamline at the European Synchrotron Radiation Facility (ESRF, Grenoble, France) for support and the facilities for allocation of beamtime.

M.D. thanks the F.R.S.-FNRS for her position as Senior Research Associate.

References

1. Nitschke, M., Costa, S.G.V.A.O., Conteiro, J., 2005. Rhamnolipid surfactants: an update on the general aspects of these remarkable biomolecules. Biotechnol. Prog.Web Release September 7, 10–13. doi: 10.1021/bp050239p
2. Lang, S., Katsiwela, E., Wagner, F., 1989. Antimicrobial effects of biosurfactants. Fat Sci. Technol. 91, 363–366. doi: 10.1002/lipi.19890910908
3. Lang, S., Wagner, F., 1993. Biological activities and applications. In: Kosaric, N. (Ed.), Biosurfactant Properties and Applications, vol. 48. Marcel Dekker, New York, pp. 251–261. ISBN 9780367402457
4. Stanghellini, M.E., Miller, R.M., 1997. Biosurfactants—their identity and potential efficacy in the biological control of zoosporic plant pathogens. Plant Dis. 81, 4–12. doi: 10.1094/PDIS.1997.81.1.4
5. J. Crouzet et al., Biosurfactants in Plant Protection Against Diseases: Rhamnolipids and Lipopeptides Case Study, 2020 Frontiers. doi: 10.3389/fbioe.2020.01014
6. Lang and Wullbrandt, Rhamnose lipids – biosynthesis, microbial production and application potential Applied Microbiology and Biotechnology volume 51, pages22–32 (1999). doi: 10.1007/s002530051358
7. Brocca et al., Interferometric investigation of the gas-state monolayer of mono-rhamnolipid adsorbing at an oil/water interface, J. Mol Liq (2018) doi: 10.1016/j.molliq.2018.06.121
8. Piljac and Piljac, 1995a. Immunological activity of rhamnolipids. US Patent 5466675.
9. Stipcevic et al., Di-rhamnolipid from Pseudomonas aeruginosa displays differential effects on human keratinocyte and fibroblast cultures, J Dermatol Sci, 2005. doi: 0.1016/j.jdermsci.2005.08.005
10. Rademann et al., Endotoxin-like properties of a rhamnolipid exotoxin fromBurkholderia(Pseudomonas)plantarii: immune cellstimulation and biophysical characterization, Biol.Chem, 2006, Vol. 387, pp. 301–310. doi: 10.1515/BC.2006.040
11. Piljac and Piljac, 1995b. Pharmaceutical preparation based on rhamnolipid. US Patent 5455232.

12. Stipcevic et al., Enhanced healing of full-thickness burn wounds using di-rhamnolipid, journal of the International Society for Burn Injuries 32(1):24-34, 2006. doi: 10.1016/j.bums.2005.07.004
13. P. Balakrishnan, S. Shanmugam, W.S. Lee, W.M. Lee, J.O. Kim, D.H. Oh, D. Kim, J.S. Kim, B.K. Yoo, H. Choi, J.S. Woo, C.S. Yong, Formulation and in vitro assessment of minoxidilniosomes for enhanced skin delivery, Int. J. Pharm. 377 (2009) 1–8. doi: 10.1016/j.ijpharm.2009.04.020
14. L. Sanchez et al., Rhamnolipids Elicit Defense Responses and Induce Disease Resistance against Biotrophic, Hemibiotrophic, and Necrotrophic Pathogens That Require Different Signaling Pathways in Arabidopsis and Highlight a Central Role for Salicylic Acid, Plant Physiol. 160 (2012) 1630. doi: 10.1104/pp.112.201913.
15. Schellenberger et al., Apoplastic invasion patterns triggering plant immunity: plasma membrane sensing at the frontline, Mol. Plant. Path. 2019, doi: 10.1111/mpp.12857
16. F. J. Aranda, M. J. Espuny, A. Marques, J. A. Teruel, A. Manresa, A. Ortiz, Thermodynamics of the Interaction of a Dirhamnolipid Biosurfactant Secreted by Pseudomonas aeruginosa with Phospholipid Membranes, Langmuir 2007, 23, 2700-2705. doi: 10.1021/la061464z
17. H. Abbasi et al., A bacterial monorhamnolipid alters the biophysical properties of phosphatidylethanolamine model membranes, Biochim. Biophys. Acta 1828 (2013) 2083. doi: 10.1016/j.bbamem.2013.04.024
18. H. Abbasi et al., Interaction of a bacterial monorhamnolipid secreted by Pseudomonas aeruginosa MA01 with phosphatidylcholine model membranes, Chem. Phys. Lip. 165(2012) 745. doi: 10.1016/j.chemphyslip.2012.09.001
19. Herzog et al. Impact of the number of rhamnose moieties of rhamnolipids on the structure, lateral organization and morphology of model biomembranes, *Soft Matter*, 2021, 17, 3191. doi: 10.1039/D0SM01934H
20. M. Sanchez, F.J. Aranda, J.A. Teruel, M.J. Espuny, A. Marques, A. Manresa, A. Ortiz, Permeabilization of biological and artificial membranes by a bacterial dirhamnolipid produced by Pseudomonas aeruginosa, J. Colloid Interface Sci. 341 (2010) 240–247. doi: 10.1016/j.jcis.2009.09.042
21. E. Haba, A. Pinazo, R. Pons, L. Pérez, A. Manresa, Complex rhamnolipid mixture characterization and its influence on DPPC bilayer organization, Biochimica et BiophysicaActa 1838 (2014) 776–783. doi: 10.1016/j.bbamem.2013.11.004
22. M. Sánchez, J.A. Teruel, M.J. Espuny, A. Marqués, F.J. Aranda, A. Manresa, A. Ortiz, Modulation of the physical properties of dielaidoylphosphatidylethanolamine membranes by a dirhamnolipid biosurfactant produced by Pseudomonas aeruginosa, Chem. Phys. Lipids (2006) 118. doi: 10.1016/j.chemphyslip.2006.04.001
23. A. Ortiz, J.A. Teruel, M.J. Espuny, A. Marqués, A. Manresa, F.J. Aranda, Effects of dirhamnolipid on the structural properties of phosphatidylcholine membranes, Int. J. Pharm. 325 (2006) 99-107. doi: 10.1016/j.ijpharm.2006.06.028
24. A. Oliva, J. A. Teruel, F. J. Aranda, A. Ortiz, Effect of a dirhamnolipid biosurfactant on the structure and phase behaviour of dimyristoylphosphatidylserine model membranes, Colloids and Surfaces B: Biointerfaces 185 (2020) 110576. doi: 10.1016/j.colsurfb.2019.110576
25. N. Monnier, A. L. Furlan, S. Buchoux , M. Deleu, M. Dauchez, S. Rippa, C. Sarazin, Exploring the Dual Interaction of Natural Rhamnolipids with Plant and Fungal Biomimetic Plasma Membranes through Biophysical Studies, Int. J. Mol. Sci. 2019, 20, 1009. doi: 10.3390/ijms20051009

26. Alessandro Prinetti, Vanna Chigorno, Laura Mauri Nicoletta Loberto Sandro Sonnino, Modulation of cell functions by glycosphingolipid metabolic remodeling in the plasma membrane, Journal of Neurochemistry, 2007, 103 (Suppl. 1), 113–125. doi: 10.1111/j.1471-4159.2007.04714.x
27. Yu, R. K., Tsai, Y. T., Ariga, T., & Yanagisawa, M. (2011). Structures, biosynthesis, and functions of gangliosides--an overview. *Journal of oleo science*, *60*(10), 537–544. doi: 10.5650/jos.60.537
28. Sipione S, Monyror J, Galleguillos D, Steinberg N and Kadam V (2020) Gangliosides in the Brain: Physiology, Pathophysiology and Therapeutic Applications. Front. Neurosci. 14:572965. doi: 10.3389/fnins.2020.572965
29. C. Schengrund, Gangliosides: glycosphingolipids essential for normal neural development and function, Trends in Biochemical Sciences (2015) Vol. 40, No. 7. doi: 10.1016/j.tibs.2015.03.007
30. S Sonnino, G Kirschner, R Ghidoni, D Acquotti, G Tettamanti, Preparation of GM1 ganglioside molecular species having homogeneous fatty acid and long chain base moieties, J Lipid Res. 1985 Feb;26(2):248-57. doi: 10.1016/S0022-2275(20)34395-9
31. L. Mauri, R. Casellato, G. Kirschner, S. Sonnino, A procedure for the preparation of GM3 ganglioside from GM1-lactone, Glycoconjugate Journal 16, 197–203 (1999). doi: 10.1023/a:1007072203345
32. V. Rondelli, P. Brocca, N. Tranquilli, G. Fragneto, E. Del Favero, L. Cantù, Building a biomimetic membrane for neutron reflectivity investigation: Complexity, asymmetry and contrast, Biophys. Chem. 2017, 229, 135–141. doi: 10.1016/j.bpc.2017.04.011
33. E. Kalb, S. Frey, L. K.Tamm, Formation of supported planar bilayers by fusion of vesicles to supported phospholipid monolayers,Biochimica et BiophysicaActa (BBA) – Biomembranes, 1103 (2) (1992) 307-316. doi: 10.1016/0005-2736(92)90101-q
34. T. Narayanan, M. Sztucki, P. Van Vaerenbergh, J. Leonardon, J. Gorini, L. Claustre, F. Sever, J. Morse and P. Boesecke, J. Appl. Cryst., 51, 1511 (2018). doi: 10.1107/S1600576718012748
35. SasView - Small Angle Scattering Analysis (2019) Available at: https://www.sasview.org/
36. Mattauch et al., The high-intensity reflectometer of the Jülich Centre for Neutron Science: MARIA, J. Appl. Cryst. 51, 646–654. doi: 10.1107/S1600576718006994
37. Koutsioubas, A. (2016). J. Phys. Chem. B, 120, 11474–11483. doi: 10.1021/acs.jpcb.6b05433
38. Helmholtz-Zentrum Berlin für Materialien und Energie. (2016). BioRef: The Reflectometer for Biological Applications (V18) at BER II. Journal of large-scale research facilities, 2, A99. doi: 10.17815/jlsrf-2-100
39. A. Nelson, Co-refinement of Multiple-contrast neutron/X-ray Reflectivity Data Using MOTOFIT, J. Appl. Crystallogr. 39, 273–276 (2006). doi: 10.1107/S0021889806005073
40. Koutsioubas, A, anaklasis: a compact software package for model-based analysis of specular neutron and X-ray reflectometry data sets, Journal of Applied Crystallography (2021) 54. doi: 10.1107/S1600576721009262
41. S. Chatterjee et al., Hydrocarbon Chain-Length Dependence of Solvation Dynamics in Alcohol-Based Deep Eutectic Solvents: A Two-Dimensional Infrared Spectroscopic Investigation*. J. Phys. Chem. B* 2019, 123, 44, 9355–9363. DOI:10.1021/acs.jpcb.oc06386
42. *Joakim P. M. Jämbeck and Alexander P. Lyubartsev, Derivation and Systematic Validation of a Refined All-Atom Force Field for Phosphatidylcholine Lipids J. Phys. Chem. B* 2012, 116, 10, 3164–3179. DOI: 10.1021/jp212503e
43. https://avogadro.cc/docs/getting-started/drawing-molecules/

44. Yun-Bin Han, Liu-Qing Chen, Zhuo Li, Yu-Meng Tan, Yan Feng, Guang-Yu Yang, Structural Insights into the Broad Substrate Specificity of a Novel Endoglycoceramidase I Belonging to a New Subfamily of GH5 Glycosidases, Journal of Biological Chemistry, Volume 292, Issue 12, 2017,4789-4800, DOI: 10.1074/jbc.M116.763821
45. http://ambermd.org/antechamber/gaff.html
46. Karl N. Kirschner et al., GLYCAM06: A generalizable biomolecular force field. Carbohydrates, J. Comp. Chem, Volume29, Issue4, (2008) 622-655. doi: 10.1002/jcc.20820
47. D.A. Case, H.M. Aktulga, K. Belfon, I.Y. Ben-Shalom, S.R. Brozell, D.S. Cerutti, T.E. Cheatham, III, V.W.D. Cruzeiro, T.A. Darden, R.E. Duke, G. Giambasu, M.K. Gilson, H. Gohlke, A.W. Goetz, R. Harris, S. Izadi, S.A. Izmailov, C. Jin, K. Kasavajhala, M.C. Kaymak, E. King, A. Kovalenko, T. Kurtzman, T.S. Lee, S. LeGrand, P. Li, C. Lin, J. Liu, T. Luchko, R. Luo, M. Machado, V. Man, M. Manathunga, K.M. Merz, Y. Miao, O. Mikhailovskii, G. Monard, H. Nguyen, K.A. O'Hearn, A. Onufriev, F. Pan, S. Pantano, R. Qi, A. Rahnamoun, D.R. Roe, A. Roitberg, C. Sagui, S. Schott-Verdugo, J. Shen, C.L. Simmerling, N.R. Skrynnikov, J. Smith, J. Swails, R.C. Walker, J. Wang, H. Wei, R.M. Wolf, X. Wu, Y. Xue, D.M. York, S. Zhao, and P.A. Kollman (2021), Amber 2021, University of California, San Francisco. doi: 10.13140/RG.2.2.15902.66881
48. A. Jakalian et al., Fast, efficient generation of high-quality atomic charges. AM1-BCC model: II. Parameterization and validation, J. Comp Chem., (2002). doi: 10.1002/jcc.10128
49. Sousa da Silva, A.W., Vranken, W.F. ACPYPE - AnteChamber PYthon Parser interfacE. BMC Res Notes 5, 367 (2012). doi: 10.1186/1756-0500-5-367
50. Mark James Abraham, Teemu Murtola, Roland Schulz, Szilárd Páll, Jeremy C. Smith, Berk Hess, Erik Lindahl, GROMACS: High performance molecular simulations through multi-level parallelism from laptops to supercomputers, SoftwareX, Volumes 1–2, 2015, Pages 19-25. doi: 10.1016/j.softx.2015.06.001
51. William L. Jorgensen*,* Jayaraman Chandrasekhar*, and* Jeffry D. Madura, Comparison of simple potential functions for simulating liquid water, J. Chem. Phys. 79, 926 (1983). doi: 10.1063/1.445869
52. G. Bussi et al., Canonical sampling through velocity rescaling, J. Chem. Phys. 126, 014101 (2007), doi: 10.1063/1.2408420
53. H. G. Petersen, Accuracy and efficiency of the particle mesh Ewald method, J. Chem. Phys. 103, 3668 (1995). doi: 10.1063/1.470043
54. B. Come, M. Donato, L. F. Potenza, P. Mariani, R. Itri, F. Spinozzi, The intriguing role of rhamnolipids on plasma membrane remodelling: From lipid rafts to membrane budding, Journal of Colloid and Interface Science, 582 (2021) 669-677. doi: 10.1016/j.jcis.2020.08.027
55. M. Sánchez, F. Aranda, M. J. Espuny, A. Marqués, J. A. Terue, Á. Manresa, A. Ortiz, Aggregation behaviour of a dirhamnolipid biosurfactant secreted by Pseudomonas aeruginosa in aqueous media, Journal of Colloid and Interface Science 307 (2007) 246–253. doi: 10.1016/j.jcis.2006.11.041
56. V. A. Bjørnestad, M. Orwick-Rydmark, R. Lund, Understanding the Structural Pathways for Lipid Nanodisc Formation: How Styrene Maleic Acid Copolymers Induce Membrane Fracture and Disc Formation, Langmuir 37, 20 (2021) 6178–6188. doi: 10.1021/acs.langmuir.1c00304

57. A.E. Blaurock, R.C. Gamble, Small phosphatidylcholine vesicles appear to be faceted below the thermal phase transition, J. Membrain Biol. 50 (1979) 187–204. doi: 10.1007/BF01868948
58. L.S. Hirst, A. Ossowski, M. Fraser, J. Geng, J. V. Selinger, R. L. B. Selinger, Morphology transition in lipid vesicles due to in-plane order and topological defects, PNAS, 110 (2013) 3242-3247. doi: 10.1073/pnas.1213994110
59. K. Komorowski, A. Salditt, Y. Xu, H. Yavuz, M. Brennich, R. Jahn, T. Salditt, Vesicle Adhesion and Fusion Studied by Small-Angle X-Ray Scattering, Biophysical Journal 114 (2018) 1908–1920. doi: 10.1016/j.bpj.2018.02.040
60. F. Pincet, T. Le Bouar, Y. Zhang, J. Esnault, J.M. Mallet, E. Perez, P. Ultraweak, Sugar-Sugar Interactions for Transient Cell Adhesion, Biophysical Journal, 80 (2001) 1354–1358. doi: 10.1016/S0006-3495(01)76108-5
61. I. Bucior, M. M. Burger, Carbohydrate–carbohydrate interactions in cell recognition, Current Opinion in Structural Biology 2004, 14:631–637. doi: 10.1016/j.sbi.2004.08.006
62. S. Hakomori, Carbohydrate-carbohydrate interaction as an initial step in cell recognition, Pure & Appl. Chem., 63 (4) (1991) 473-482. doi: 10.1351/pac199163040473
63. J. C. Morales, D. Zurita, S. Penadés, Carbohydrate−Carbohydrate Interactions in Water with Glycophanes as Model Systems, J. Org. Chem. 1998, 63, 25, 9212–9222. doi: 10.1021/jo9807823
64. B. Kav, A. Grafmüller, E. Schneck, T. R. Weikl, Weak carbohydrate–carbohydrate interactions in membrane adhesion are fuzzy and generic, Nanoscale, 2020, 12, 17342. doi: 10.1039/D0NR03696J
65. I. Bucior, S. Scheuring, A. Engel, M. M. Burger, Carbohydrate–carbohydrate interaction provides adhesion force and specificity for cellular recognition, J Cell Biol. 2004 May 24; 165(4): 529–537. doi: 10.1083/jcb.200309005
66. D. Spillmann, M. M. Burger, Carbohydrate-carbohydrate interactions in adhesion, Journal of Cellular Biochemistry 61 :562-568 (1996). doi: 10.1002/(sici)1097-4644(19960616)61:4<562::aid-jcb9>3.0.co;2-m
67. Hakomori S, Handa K, Iwabuchi K, Yamamura S, Prinetti A (1998) New insights in glycosphingolipid function: “glycosignaling domain,” a cell surface assembly of glycosphingolipids with signal transducer molecules, involved in cell adhesion coupled with signaling. Glycobiology 8:xi–xix. doi: 10.1093/oxfordjournals.glycob.a018822
68. T. T. Nguyen, I. Rouzina, and B. I. Shklovskii, Reentrant condensation of DNA induced by multivalent counterions, J. Chem. Phys. 112, 2562 (2000). doi: 10.1063/1.480819
69. T. Mukhina, A. Hemmerle, V. Rondelli, Y. Gerelli, G. Fragneto, J. Daillant, T. Charitat, Attractive Interaction between Fully Charged Lipid Bilayers in a Strongly Confined Geometry, J. Phys. Chem. Lett. 2019, 10, 22, 7195–7199. doi: 10.1021/acs.jpclett.9b02804